Title

Electromagnetic induction in a conductive strip in a medium of contrasting conductivity: application to VLF and MT above molten dykes

Journal

Geophysical Journal International, 199(2)

ISSN

0956-540X

Author

Davis, Paul M

Publication Date

2014-09-23

DOI

10.1093/gji/ggu320

Peer reviewed

Electromagnetic induction in a conductive strip in a medium of contrasting conductivity: Application to VLF and MT above molten dikes.

Paul M. Davis

September 15, 2014

Abstract: Very low frequency (VLF) electromagnetic waves that penetrate conductive magma-filled dikes generate secondary fields on the surface that can be used to invert for dike properties. The model used for the interpretation calculates currents induced in a conductive strip by an inducing field that decays exponentially with depth due to the conductivity of the surrounding medium. The differential equations are integrated to give an inhomogeneous Fredholm equation of the second kind with a kernel consisting of a modified Bessel function of the second kind. Numerical methods are typically used to solve for the induced currents in the strip. In this paper we apply a modified Galerkin-Chebyshev method, which involves separating the kernel into source and field spectra and integrating the source terms to obtain a matrix equation for the unknown coefficients. The incident wave is expressed as a Chebyshev series. The Modified Bessel function is separated into a logarithmic singularity and a non-singular remainder, both of which are expanded in complex Chebyshev polynomials. The Chebyshev coefficients for the remainder are evaluated using a fast Fourier transform, while the logarithmic term and incident field have analytic series. The deconvolution then involves a matrix inversion. The results depend on the ratio of strip-size to skin-depth. For infinite skin-depth and a singular conductivity distribution given by $\tau_0 a/\sqrt{a^2 - z^2}$ (where τ_0 is the conductance, a is the half-length, and z the distance from the center), Parker (2011) gives an analytic solution. We present a similar analytic series solution for the finite skin-depth case, where the size to skin depth ratio is small. Results are presented for different ratios of size to skin depth that can be compared with numerical solutions. We compare full-space and half-space solutions. A fit of the model to VLF data taken above a magma filled dikes in Hawaii

and Mt Etna demonstrates that while properties such as depth to top, conductivity ratio, tilt, and dip can be determined, the depth to bottom is indeterminate due to the exponential decay of the inducing field.

1 Introduction

When a magma intrudes the surrounding country rock it generates an electromagnetic contrast that can have orders of magnitude higher conductivity than the surroundings (Zablocki 1976, Kauahikaua et al., 1998). Secondary fields induced by very low frequency (VLF) or high-frequency magnetotelluric waves (MT) generate fields at the surface that can be used to provide information on the underground magmatic state. In Hawaii, magma intrudes into dikes that are fed by magma chambers. The location and geometry of newly formed dikes can be estimated using VLF (Zablocki 1976, 1978), and whether the dikes remain molten, since the conductivity decreases by several orders of magnitude on solidification. Provided measurements are not taken near the ends the problem is two-dimensional, and a single conductivity contrast between the dike and country rock is an adequate approximation.

Numerical schemes for solving magnetotelluric problems are well-developed, e.g., integral equation (Hohmann 1971), finite differences and elements (Weaver et al., 1985, 1986; Wannamaker et al., 1987; Key and Weiss, 2006). The equations can become quite complicated. Hohmann (1971) describes a numerical method for solving two-dimensional problems and an associated FORTRAN program (SCATPW.F90 Anderson et al., 1976) has been used for analysis of Hawaii data (Zablocki, 1976, 1978). The program uses a collocation method to invert for currents in the conductive body and takes into account the decay of the inducing field in the surrounding conductive half-space as well as the free-surface boundary conditions. In that the method involves Green's functions that are fairly complex, involving singularities and infinite integrals, it is useful to have analytic solutions for end-members against which the numerical method can be compared. In addition, such simple solutions give insight on the dependence of the electromagnetic response to skin depth and size.

Analytical solutions to VLF or MT problems are rare and have been applied to end-member models bounded by strata of infinite or zero conductivity (Rankin, 1962, Parker 2011). Rankin (1962) solved for a dike of finite width between layers of infinite or zero conductivity. Parker (2011) presented an analytic solution for the conductive strip in a uniform magnetic field for the case where the dike is modeled by a thin strip that lies on an infinite conductivity substratum. The matrix either side of the strip has zero conductivity, and so the incident field is determined by displacement currents.

The strip used by Parker (2011) has a singular conductivity distribution $\tau_0 a/\sqrt{a^2 - z^2}$. It corresponds to a thin vertical conductive ribbon extending above a perfectly conducting half space subjected to a constant B field in the horizontal direction. It could be used, for example, to model a dike intruding conducting sediments, if the lower

end of the dike was rooted in high conductivity magma, and the sediments had a low enough conductivity that the skin depth for the frequency of incident radiation was large. The applied constant B field gives rise to an E field that varies linearly with depth. The solution for the induced current in the dike is rather simple, taking the form of a ramp function in depth. However, for the VLF method, induced currents in the surrounding medium dominate over displacement currents. These cause the incident B and E fields to have a spatial distribution that decays exponentially with the skin-depth (e.g., 300 m), and so a more extended model than the constant B field case is required, which we develop here following Parker's procedure. In section 2 we treat the full-space problem for which simple solutions can be derived. In section 3 we we compare it with the half-space problem.

2 Full-Space Model

2.1 Governing Equations

For the range of frequencies used in magnetotellurics and VLF, and conductivities in the Earth, we can ignore displacement currents, and assume the permeability and permittivity contrasts are zero, with representative values of μ_0, ϵ_o respectively (Telford et al., 1990). The induced currents are due to the contrast in conductivity $\sigma_2 - \sigma_1$, where σ_2 is the conductivity of the strip and σ_1 that of the surrounding medium. Maxwell's equations become

$$\nabla \times E = -\dot{B} \tag{1}$$

$$\nabla \times H = \sigma E \tag{2}$$

Let $B = B_0 \exp(i\omega t) = \mu_0 H_0 \exp(i\omega t)$

$$\nabla \times E = -i\omega\mu_0 H_0 \tag{3}$$

$$\nabla^2 E = i\omega\mu_0\sigma E = k^2 E \tag{4}$$

$$\nabla^2 H = i\omega\mu_0\sigma H = k^2 H \tag{5}$$

where $k = \sqrt{i\omega\sigma\mu_0}$. We choose the magnetic field at the surface to be in the $x-$ direction. The dike lies in the $y - z$ plane as in Figure (1) and can have a dip at angle

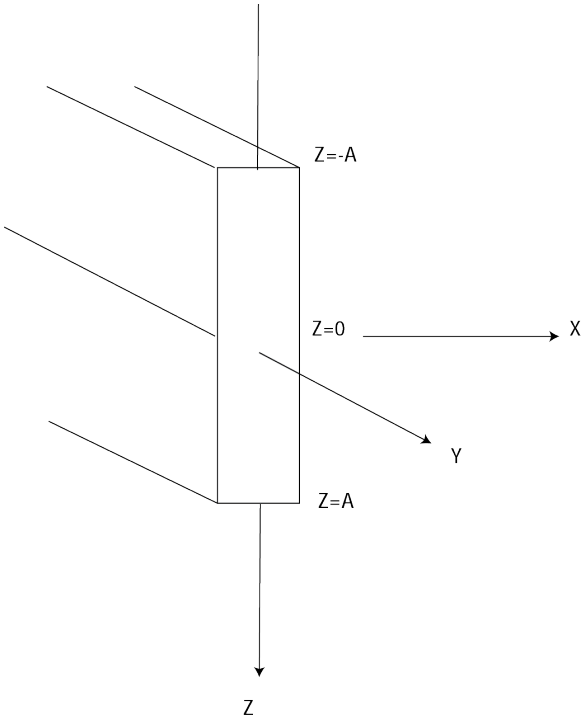

Figure 1: Geometry

θ with the horizontal. All currents are in the y−direction. Let the incident field be $E_y^i = E_0 \exp(i\omega t)$ and the skin depth

$$\delta_1 = (\frac{2}{\omega \mu_0 \sigma_1})^{1/2} \tag{6}$$

The solution for the incident field at depth is given by

$$E_y^i = E_0 \exp(-k_1 z) = E_0 \exp(-(i+1)z/\delta_1) \tag{7}$$

(e.g., Telford et al., 1990) with a similar expression for H that can be derived using Eq. (1). Equation (4) within and outside the strip becomes

$$\nabla^2 E_2 = k_2^2 E_2 \tag{8}$$

$$\nabla^2 E_1 = k_1^2 E_1 \tag{9}$$

We separate the total field E_y in the strip into the incident field E_y^i and the scattered field E_s generated by the induced currents J_s in the strip, i.e.,

$$E_y = E_y^i + E_s \tag{10}$$

Substituting in Eqs. (8,9) the differential equations for E_y and E_y^i become, respectively:

$$\nabla^2 (E_y^i + E_s) = k_2^2 (E_y^i + E_s) \tag{11}$$

$$\nabla^2 E_y^i = k_1^2 E_y^i \tag{12}$$

Eqs.(11,12) represent two coupled partial differential equations for a given E_y^i. If we subtract $k_1^2 E_y$ from Eq.(11)

$$\nabla^2 E_y - k_1^2 E_y = k_2^2 E_y - k_1^2 E_y \tag{13}$$

$$\nabla^2 E_y - k_1^2 E_y = i\omega \mu_0 (\sigma_2 - \sigma_1) E_y \tag{14}$$

$$\nabla^2 E_y - k_1^2 E_y = i\omega \mu_0 J_S \tag{15}$$

Subtracting Eq (12) gives

$$\nabla^2 E_s - k_1^2 E_s = i\omega\mu_0 J_S \tag{16}$$

Eq.(16) is a second order differential equation for the scattered field generated by a distribution of current embedded in a medium of conductivity σ_1. The scattering current is confined to the inhomogeneity. To obtain a solution to Eq.(16) we multiply by the Green's function $G_0(x, z; x'z')$, which gives the electric field at (x, z) for unit current located at (x', z') , and integrate over the cross-section (Hohmann, 1971) to obtain

$$E_s(x, z) = \iint_{S'} \{[\sigma_2(x'z') - \sigma_1]E_y(x'z')G_0(x, z; x'z')dx'dz' \tag{17}$$

and from Eq.(10)

$$E_y(x, z) = E_y^i(x, z) + \iint_{S'} \{[\sigma_2(x'z') - \sigma_1]E_y(x'z')G_0(x, z; x'z')dx'dz' \tag{18}$$

with

$$G_0(x, z; x', z') = \frac{-i}{\pi\delta_1^2\sigma_1} K_0\left(\frac{(1+i)}{\delta_1}[(x-x')^2 + (z-z')^2]^{1/2}\right) \tag{19}$$

(Wait, 1962) where K_0 is the modified Bessel function of the second kind of order zero. Eq. (18) is a singular, inhomogeneous, Fredholm, integral equation of the second kind for E_y.

We approximate a thin dike by a strip of uniform conductivity of half height a, and width w ; Eq. (18) becomes

$$E_y(x, z) = E_y^i(z) + w[\sigma_2 - \sigma_1] \int_{-a}^{a} E_y(x', z')G_0(x, z; x', z')dz' \tag{20}$$

Following Hohmann (1971) effects of frequency, conductivity and permeability can be taken into account by expressing dimensions in skin depths Eq.(6). Letting $Z = z/\delta_1$ and $W = w/\delta_1$, $A = a/\delta_1$. Substituting these in Eq. (20) it becomes

$$E_y(X, Z) = E_y^i(Z) + W[\sigma_2 - \sigma_1]\delta_1^2 \int_{-A}^{A} E_y(X', Z')G_0(X, Z; X', Z')dZ' \tag{21}$$

Letting

$$G(X,Z;X',Z') = K_0\{(1+i)[(X-X')^2+(Z-Z')^2]^{1/2}\} \tag{22}$$

and substituting for G_0 from Eq.(19), Eq.(21) becomes

$$E_y(X,Z) = E_y^i(X,Z) - \frac{i\Omega}{A}\int_{-A}^{A} E_y(Z')G(X,Z;X',Z')dZ' \tag{23}$$

with

$$\Omega = \frac{WA}{\pi}[\frac{\sigma_2}{\sigma_1} - 1] \tag{24}$$

(Wait, 1962, Erdelyi, 1954, see Eqs.(17, 23) Hohmann). This type of equation has been solved numerically by evaluating the convolution at digitized field and source points (Hohmann 1971; Anderson et al., 1976, with FORTRAN program SCATPW.F) where the Green's function also includes an extra term that models effects of surface reflections.

2.2 General Solution

We use the Galerkin-Chebyshev matrix method (Cole, 1998, Boyd, 2001, slightly modified in that we expand the integral equation in Chebyshev polynomials rather than polynomials divided by the sin of the angle) to solve Eq.(22) by expanding it in Chebyshev polynomials and solving for coefficients. We separate the integrand into field and source points using a similar approach to that used by Parker (2011). For a conductive strip dipping at angle θ with respect to the X-axis, let $Z = A\cos(\varphi),\ X = Zcot(\theta)$ and $Z' = A\cos(\psi),\ X' = Z'cot(\theta)$. We expand E_y and E_y^i in Chebyshev series, i.e.,

$$E_y = \sum_{l=0}^{\infty} E_l \cos(l\psi) = E_l T_l(\psi) \tag{25}$$

$$E_y^i = \sum_{n=0}^{\infty} E_n^i \cos(n\varphi) = E_n^i T_n(\varphi) \tag{26}$$

where T_n are Chebyshev polynomials of the first kind, and the summation convention for repeated indices applies. The Green's function can be expanded as

$$G(X,Z;X',Z') = \sum_{n=0}^{\infty}\sum_{m=0}^{\infty} G_{nm}\cos(n\varphi)\cos(m\psi) = G_{nm}T_n(\varphi)T_m(\psi) \tag{27}$$

where

$$G_{nm} = \int_0^{\pi}\int_0^{\pi} G(\cos\varphi;\cos\psi)\cos(n\varphi)\cos(m\psi)d\varphi d\psi \tag{28}$$

Equation 22 becomes

$$\begin{aligned}&\sum_{n=0}^{\infty} E_n\cos(n\varphi) = \sum_{n=0}^{\infty} E_n^i\cos(n\varphi) + \\ &i\Omega\int_{\pi}^{0}\sum_{l=0}^{\infty} E_l\cos(l\psi)\sum_{n=0}^{\infty}\sum_{m=0}^{\infty} G_{nm}\cos(n\varphi)\cos(m\psi)\sin\psi d\psi\end{aligned} \tag{29}$$

which, on reversing the integral and using the Einstein summation convention, becomes,

$$E_nT_n(\varphi) = E_n^iT_n(\varphi) - i\Omega G_{nm}T_n(\varphi)\int_0^{\pi} T_m(\psi)T_l(\psi)\sin\psi d\psi E_l \tag{30}$$

The integrals in ψ can be evaluated as

$$A_{ml} = \int_0^{\pi}\cos(m\psi)\cos(l\psi)\sin\psi d\psi \tag{31}$$

$$\begin{aligned}A_{ml} &= \frac{1-m^2-l^2}{(l+m+1)(l+m-1)(l-m+1)(l-m-1)} \qquad (m+l+1 \quad odd)\\ &= 0 \qquad\qquad\qquad\qquad\qquad\qquad\qquad\qquad\qquad\qquad (m+l+1 \quad even)\end{aligned} \tag{32}$$

The integral equation then becomes

$$E_nT_n = E_n^iT_n - i\Omega G_{nm}T_nA_{ml}E_l \tag{33}$$

Collecting terms

$$E_n = E_n^i - i\Omega G_{nm} A_{ml} E_l \tag{34}$$

The solution is given by the matrix inversion

$$E_l = [I + i\Omega G_{nm} A_{ml}]^{-1} E_n^i \tag{35}$$

Provided the G_{nm} can be calculated, the solution is obtained with an accuracy depending on the number of coefficients. However the G_{nm} contain a logarithmic singularity and so the integrals in Eq. (28) are not straightforward. Therefore we decompose the kernel into the logarithmic component, that has a Chebyshev series, and the smooth remainder, for which the series may be obtained analytically, or numerically using the fast Fourier transform.

The modified Bessel function of the Green's function, (Eq.24), $G(|A\cos\varphi - A\cos\psi|) = K_0(|A\cos\varphi - A\cos\psi|\,(1+i))$ can be expanded (Abramowitz and Stegun, 1977, 9.6.13, Cope 1998) as

$$\begin{aligned} G(|A\cos\varphi - A\cos\psi|) = \sum_{k=0}^{\infty} \frac{(1+i)^{2k}}{4^k (k!)^2} (&- \log|A\cos\varphi - A\cos\psi| + \\ &\log\sqrt{2} - \gamma - \frac{\pi}{4} i + a_k) \times |A\cos\varphi - A\cos\psi|^{2k} \\ a_0 = 0 \quad a_k = 1 + 1/2 + ... + 1/k \quad &(k > 0) \end{aligned} \tag{36}$$

where γ is Euler's constant = 0.577215664. The logarithmic singularity contained in Eq. (36) has a Chebyshev expansion given by

$$\begin{aligned} -\log((1+i)\,|A\cos\psi - A\cos\varphi|) &= L_{00} + \sum_{1}^{N} \frac{2}{n} \cos(n\varphi)\cos(n\psi) \\ &= L_{nm} T_n(\varphi) T_n(\psi) \end{aligned} \tag{37}$$

with

$$\begin{aligned} L_{nm} &= \log\left\{ 2\frac{\sqrt{2}}{A} \exp(-\gamma) \right\} - i\pi/4 \qquad n = 0 \\ &= \frac{2}{n} \qquad\qquad\qquad\qquad\qquad\qquad\quad n > 0 \end{aligned} \tag{38}$$

The remaining terms in $|\cos\varphi - \cos\psi|$ are also separable. Thus each of the terms in Eq.(22) is separable and can be integrated over ψ to obtain the G_{nm} as a series (See

Cope 1998, who uses recurrence relations to minimize computations). To separate out the singularity we decompose the Green's function into the logarithmic term and remainder given by,

$$R(|A\cos\varphi - A\cos\psi|) = K_0(A\,|\cos\varphi - A\cos\psi|\,(1+i))+ \\ \log((1+i)\,|A\cos\psi - A\cos\varphi|) \tag{39}$$

Then the

$$G_{nm} = (R_{nm} + L_{nm}\delta_{nm}) \tag{40}$$

where R_{nm} is the double Chebyshev transform of R. For our purposes we use an FFT to compute the R_{nm} (We used Von Winckel's, 2004 MATLAB program for the 2D Chebyshev transform). For a given half- length A, R_{nm} is evaluated at $N+1$ Chebyshev-Gauss-Lobatto points $\psi_n = n\pi/N$, $\phi_n = n\pi/N$, $n = 0...N$, and fast Fourier transformed to obtain the R_{mn}. A value of N=40 was used for the case discussed below. Eq. (35) becomes,

$$E_l = [I + i\Omega(\delta_{nm}L_{nm} + R_{nm})A_{ml}]^{-1}E_n^i \tag{41}$$

For an incident field E_y^i we need to calculate its Chebyshev coefficients E_n^i . Consider an E field at the surface which exponentially decays to a strength strength E_0 at the center of the dike. Equation (7) can be written

$$E_y^i = E_0\exp(-(i+1)A\cos\varphi) = E_0\sum_{n=0}^{\infty}(-1)^n i^n\gamma_n J_n((1-i)A)\cos(n\varphi) \\ \gamma_n = 1 \qquad n = 0 \\ \gamma_n = 2 \qquad n > 0 \tag{42}$$

Therefore the Chebyshev coefficients for the exponentially decaying wave are

$$E_n^i = E_0(-1)^n i^n\gamma_n J_n((1-i)A) \tag{43}$$

Figure 1 shows the test strip. It has a width of 1 m and a length of 100 m. An incident E field given by Eq. (7) is applied at the surface which has a value $E_0 = 1$ at the center of the strip. The frequency used was 20,000Hz. The conductivity of the strip $\sigma_2 = 1$ S/m. The conductivity of the matrix σ_1 was varied to correspond to skin depths of 36 km, 356, 113, 36, 11 and 1 meters. Corresponding real and imaginary components of the induced field are plotted in Figs. (2a-2f) respectively. The stars are points calculated from the Numerical solution (Hohmann, 1971, but setting the surface terms in

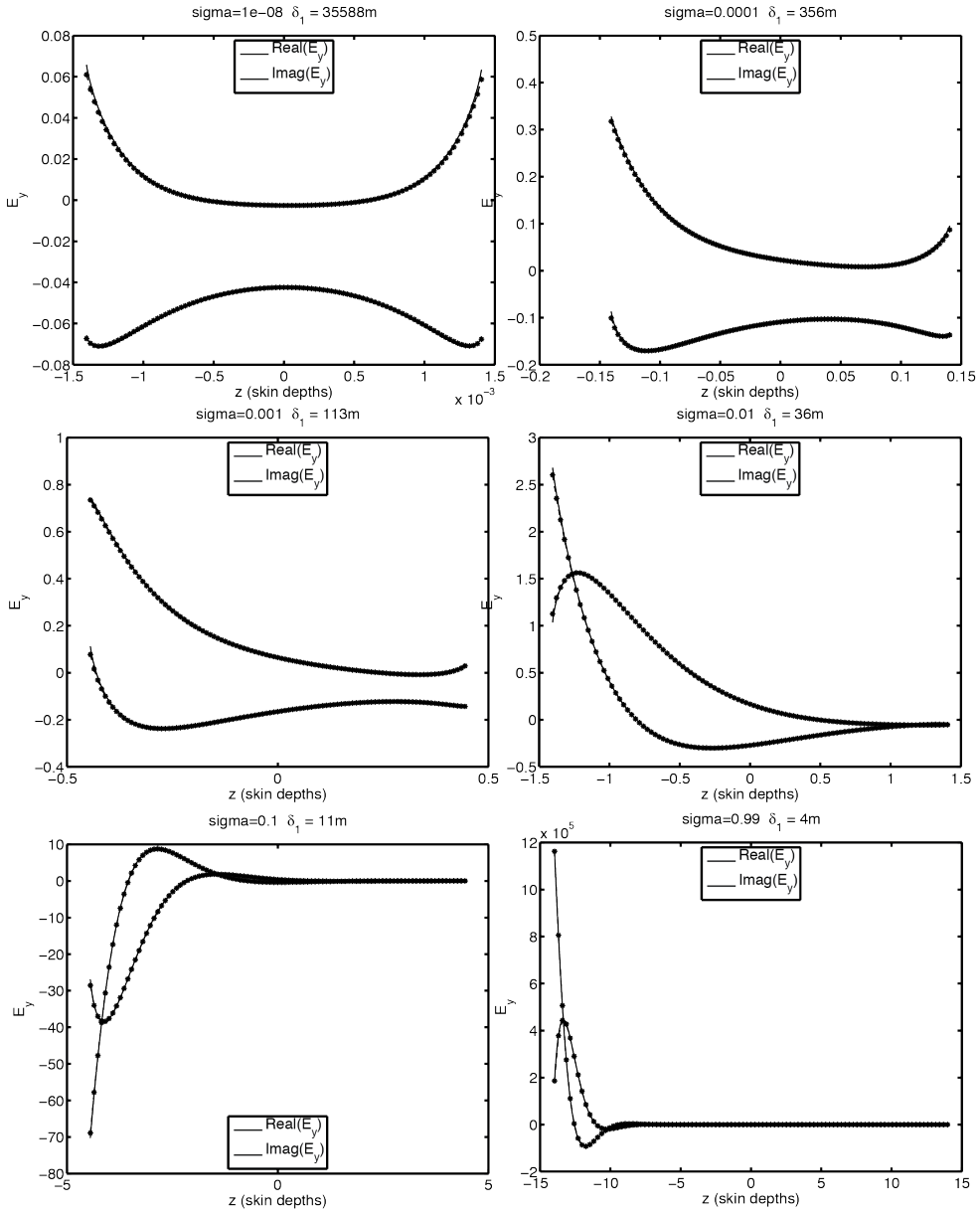

Figure 2: Real and imaginary E_y for different skin depths (Lines) calculated using Eq. (41). Stars are numerical solutions using a MATLAB version of the FORTRAN program SCATPW.F90 described by Anderson et al., (1976).

the program SCATPW.F90 to zero). At large skin depth the incident field is almost uniform and the induced fields are curved and symmetrical. As skin depth decreases, the effect of the decay in the inducing field with depth becomes apparent. When the skin depth is a small fraction of the dike length, the results become independent of the lower boundary. In such cases, the secondary field cannot be used to detect the overall dimensions of the dike, but are useful for depth of the top, lateral position, dip, and the product of conductivity contrast and width - which determines amplitude.

2.3 The infinite skin depth case

When the surrounding medium has zero conductivity,

$$G_0(z;z') = \frac{-i\omega\mu_0}{2\pi}\log(|z-z'|) \tag{44}$$

A constant B field, as solved by Parker (2011) applies, as in this case displacement currents become relevant. The incident E field is given by $E_y^i = i\omega B_0 z$. Using the same conductance distribution as Parker (2011), i.e., $\tau_0 a/\sqrt{a^2-z^2}$, and taking into account finite-width, the conductivity becomes, $\sigma_2 = \tau_0 a/w\sqrt{a^2-z^2}$. Equation (20) is then

$$E_y(z) = E_y^i(z) - \frac{i\omega\mu_0\tau_0}{2\pi}\int_{-a}^{a} E_y(z')\log(|z-z'|)a/\sqrt{a^2-z'^2}dz' \tag{45}$$

Transforming to coordinates (φ,ψ) and taking the Chebyshev transform

$$\cos\varphi = z/a, \cos\psi = z'/a \tag{46}$$

$$\begin{aligned} E_nT_n(\varphi) &= E_n^iT_n(\varphi) - i\frac{\omega\mu_0\tau_0 a}{2\pi}T_n(\varphi)L_n\int_0^{\pi}T_n(\psi)T_l(\psi)d\psi E_l \\ L_n &= \log\frac{2}{A} \qquad n=0 \\ &= \frac{2}{n} \qquad n>0 \end{aligned} \tag{47}$$

For the Chebyshev spectral expansion, the chosen conductivity distribution is the weight function for the orthogonality condition for Chebyshev polynomials $a/\sqrt{(a^2-}$

$z^2) = 1/sin\psi$. After evaluating the integrals, only the $n = l$ terms remain, and Eq. (47) becomes

$$\begin{aligned} E_n T_n(\varphi) &= E_n^i T_n(\varphi) - i\frac{\omega\mu_0\tau_0 a}{2\pi} T_n(\varphi) L_n N_n E_n \\ N_n &= \pi \qquad\qquad n = 0 \\ N_n &= \pi/2 \qquad\qquad n \neq 0 \end{aligned} \tag{48}$$

We equate the coefficients of Chebyshev polynomials to obtain

$$E_n = E_n^i - \frac{i\omega\mu_0\tau_0 a}{2\pi} N_n E_n L_n \tag{49}$$

rearranging gives,

$$E_n = \frac{E_n^i}{1 + \frac{1}{2\pi} i\omega\mu_0\tau_0 a L_n N_n} \tag{50}$$

For the uniform B field where $E = i\omega B_0 z$, $n = 1$ and $L_n = L_1 = 2$, $N_1 = \pi/2$.

$$E_1 = \frac{i\omega B_0}{1 + \frac{1}{2} i\omega\mu_0\tau_0 a} \tag{51}$$

which is Parker's (2011) equation (14).

Noting from Eq.(51) that τ_0 is conductivity times width at $z = 0$, we let this conductivity be $\sigma = \tau_0/w$. The skin-depth in a strip of this conductivity is then $\delta_2 = (2/\omega\mu_0\sigma)^{1/2}$. Eq. (51) becomes

$$E_1 = \frac{i\omega B_0}{1 + 1/2 i\omega\mu_0 w\sigma a} = \frac{i\omega B_0}{1 + i\omega a/\delta_2^2} = \frac{\pi B_0}{\pi + iWA} \tag{52}$$

and the more general Eq. (50) becomes

$$E_n = \frac{E_n^i}{1 + \frac{iN_n L_n w a}{\pi\delta_1^2}} = \frac{\pi E_n^i}{\pi + iN_n L_n WA} \tag{53}$$

that is, the dimensionless term in the denominator is the cross-sectional area of the strip expressed in units of skin-depth squared.

2.4 The finite skin depth case

We examine next the intermediate case for which the skin depth is larger (e.g., several times) than the dimensions of the strip, but not necessarily infinitely larger, and induced currents dominate over displacement currents. Then the kernel takes the form of the complex logarithm that can be expanded to include a complex offset term and the Chebyshev series in Eq. (37). That is, the R_{nm} terms in Eqs(40,41) become second order and the G_{nm} are analytic. The Green's function can be approximated as

$$\begin{aligned} K_0(|Z'-Z|\,(1+i)) &= -\log|Z'-Z| + \log\sqrt{2} - \gamma - \frac{\pi}{4}i + ... \\ &= \log\left\{2\frac{\sqrt{2}}{A}\exp(-\gamma)\right\} - i\frac{\pi}{4} + 2\sum_{1}^{N}\frac{1}{n}\cos(n\varphi)\cos(n\psi) \end{aligned} \tag{54}$$

Then the solution becomes

$$E_l = [I + i\Omega L_{nn} A_{nl}]^{-1} E_n^i \tag{55}$$

where the L_{nn} are given in Eq.(38). Figure 3 shows that for δ_1/A large this approximation gives a good fit, but when the ratio approaches unity Eq. 35 is required.

2.5 Strip with infinite conductivity

Another case with an analytic solution (e.g., Brant, 1992), against which our method may be tested is that of the infinitely conductive dike in a uniform magnetic field applied normal to its axis.

$$E_y = \frac{2zH_0}{\sigma(a^2 - z^2)^{1/2}} \tag{56}$$

Our program reproduces this case, but near the singularities at the ends the solutions exhibit the Gibb's phenomenon.

As a final check equations (11,12) were solved by iterative finite differences based on the successive over/under relaxation method. We can thus arrive at the solutions using three methods (1) numerical (2) Galerkin-Chebyshev and (3) finite differences, all of which serve as mutual checks and in some cases simple analytical formulae can be extracted. The range of solutions presented in this paper and the regimes over which they apply are listed in Table 1.

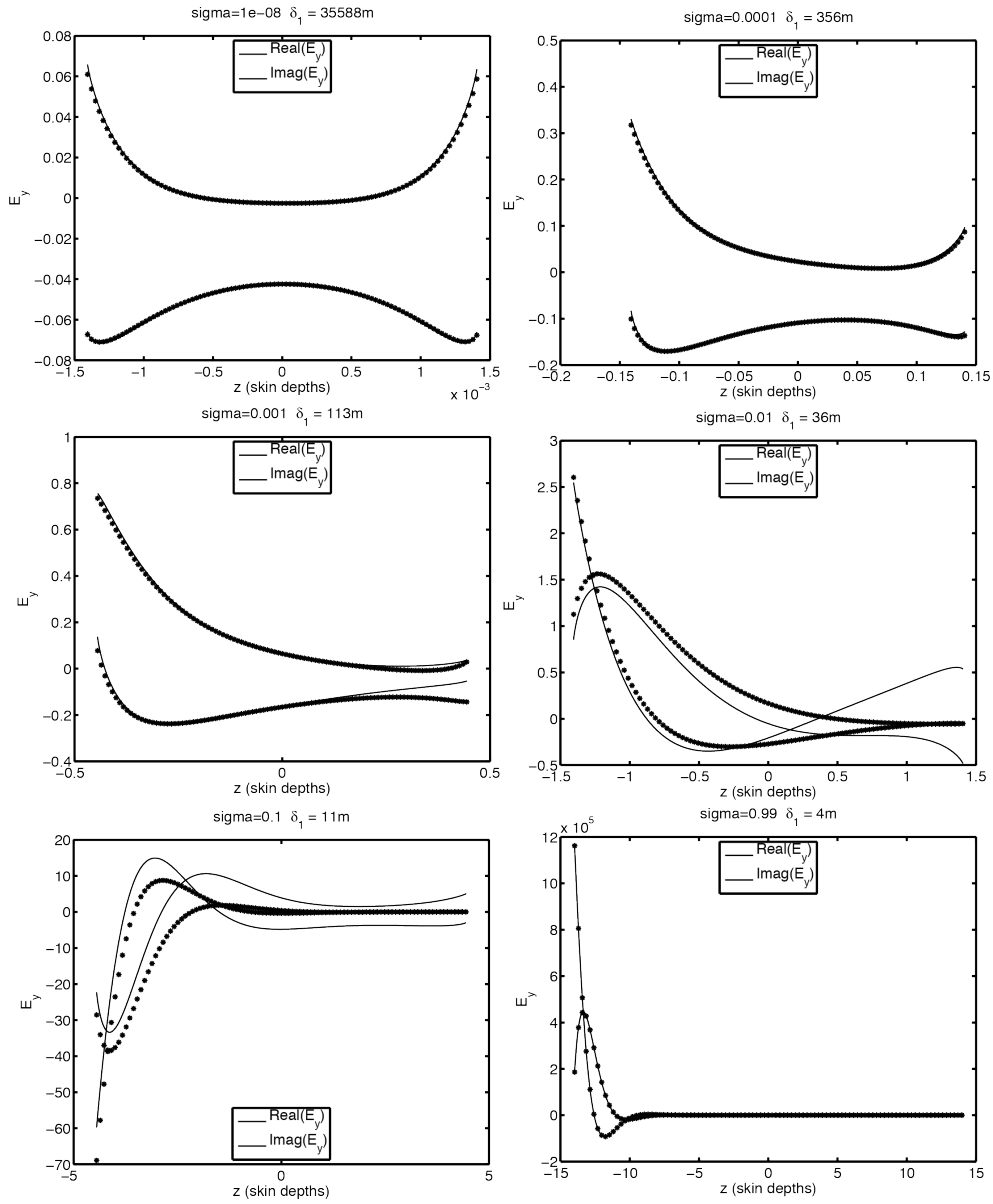

Figure 3: As in Figure (2) but using the approximate Green's Function Eq.(55). The stars are numerical values. The analytic series are plotted as lines. The approximate solution applies for the case where skin depth is larger than the body (here 100 m in length) as the misfit in the lower figures shows.

Matrix Cond. σ_1	Strip Cond. σ_2	skin depth δ_1	E_l , ${}^1E(z)$	Eq No.
all	all	all	$[I + i\Omega G_{nm}A_{ml}]^{-1}E^i_n$	Eq.(35)
all	all	>A	$[1 + i\Omega L_{nn}A_{nl}]^{-1}E^i_n$	Eq.(55)
0	$\frac{\tau_0 a}{w\sqrt{a^2-x^2}}$	∞	$[\pi + iWA]^{-1}\pi B_0$	Eq.(52)
0	$\frac{\tau_0 a}{w\sqrt{a^2-x^2}}$	∞	$[\pi + iN_nL_nWA]^{-1}\pi E^i_n$	Eq.(53)
0	∞	∞	${}^1E(z) = 2zH_0/(a^2 - z^2)^{1/2}/\sigma$	Eq.(57)

Table 1. Analytic spectral solutions for the conductive strip. The second case Eq.(55) applies to strip buried in a weakly conductive earth. The $\sigma_1 = 0$ cases correspond to a strip in a vacuum. The singular conductivity function corresponds to that used by Parker (2011).

3 Half-Space Model

3.1 Governing Equations

In this section we use the Galerkin-Chebyshev method to solve the problem for a buried, dipping dike in a conductive half space. The full solution to the underground dike problem requires an extra term in the Green's function to satisfy surface boundary conditions. The full-space Green's function Eq. (19, 24) is expanded as an integral of plane waves, for which plane wave reflection coefficients give the reflected fields from the surface that are superposed on the direct field (Wait, 1962). For example, for the E_y field the Green's function is,

$$G^{EY}_s(X, Z; X', Z') = \int_0^\infty \frac{u-g}{u+g}\frac{e^{-u(Z+Z')}}{u} cos[g(X - X')]dg \tag{57}$$

where $u = (g^2 + 2i)^{1/2}$. The resulting integrals require time-consuming numerical integration. In order to calculate the surface field contributions just once, we divide the $X - Z$ space of interest into Chebyshev-Gauss-Lobatto nodes, and calculate the two-dimensional Chebyshev spectrum $G^{EY}_s(cos(n\varphi), cos(m\psi))$, which is used to evaluate the surface fields at arbitrary [$X - X'$,$Z + Z'$]. The G^{EY}_s is nonsingular and can be added to the remainder values R_{nm} in Eq.(39) and thus Eq. (41) is the required solution for the induced fields in the strip.

In order to calculate the field on the surface, the induced field is then convolved with the appropriate Green's functions to obtain the surface magnetic and electric fields, from which tilt and ellipticity can be calculated, as well as surface impedance. The convolution may be written

$$F(X) = \int_{-A}^{A} E_y(X', Z') G^F(X, X'; Z, Z') dZ' \tag{58}$$

where F is the $[HX, HZ, EY]$-field at the surface when the corresponding Green's function G^F is used. In general the G^F have terms that include surface reflections as well as source effects (Hohmann, 1971). We take the two-dimensional Chebyshev spectrum at the Chebyshev-Gauss-Lobatto points, where φ corresponds to points along the surface and ψ to those along the strip, and perform the convolution as in Eqs.(19) and (33),

$$F_i = G^F_{ij} A_{jl} E_l \tag{59}$$

where F_n is the n'th term in the Chebyshev expansion of the field on the surface. Shifting the origin such that $Z = 0$ is on the surface, the G^F are as follows,

$$\begin{aligned}
G^{HX}(X, 0; X', Z') &= (1+i) H_0 \Omega \sigma_1 \Big\{ \frac{Z'}{2R} K_1\{(1+i)R\} + \\
&\qquad \int_0^\infty \frac{g-u}{g+u} e^{-uZ'} cos[g(X-X')] dg \Big\} \\
G^{HZ}(X, 0; X', Z') &= (1+i) H_0 \Omega \sigma_1 \Big\{ \frac{X-X'}{2R} K_1\{(1+i)R\} \\
&\qquad \int_0^\infty \frac{u-g}{u+g} \frac{g}{u} e^{-uZ'} sin[g(X-X')] dg \Big\} \\
G^{EY}(X, 0; X', Z') &= i H_0 \Omega \delta_1 \Big\{ K_0\{(1+i)R\} \\
&\qquad \int_0^\infty \frac{u-g}{u+g} \frac{e^{-uZ'}}{u} cos[g(X-X')] dg \Big\}
\end{aligned} \tag{60}$$

where $R = [(X - X')^2 + Z'^2]^{1/2}$ and second terms are surface reflections. The full

solution, combining Eq.(41) and (58) becomes

$$F_i = G^F_{ij} A_{jl} \frac{E^i_n}{[I + i\Omega(\delta_{nm} L_{nm} + R_{nm}) A_{ml}]} \tag{61}$$

where G^F_{ij} is given by Eq.(60), E^i_n by Eq.(43), L_{nm} by Eq.(38), R_{nm} by the Chebyshev transform of Eq.(39) plus Eq.(58), A_{nm}, and A_{jl} by Eq.(32).

3.2 Numerical Comparison

The solution for the full-space problem including all surface reflections in the Green's functions G_{mn} and G_{Fmn} for surface fields $F = [E_y, H_x, H_z]$ tilt, ellipticity and impedance using Eqs. (41 and 58) are shown in Figures (4-8). The model chosen is similar to one published by Zablocki, (1976), i.e., $\sigma_1 = 0.0001, \sigma_2 = 1$ S/m, Depth=30 m, Width=1 m, Length=25 m, but with a dip of 60^o. For a dip of 90^o our solutions are identical to those published. Stars are numerical solutions using a MATLAB version of SCATPW.F90. Solid lines are half-space solutions including surface terms. Dashed lines use the approximate Eq(41), that do not include the effects of the surface reflections. For this case the dimensions are sufficiently small compared with the skin depth that Eq.(55) gives near identical results. We found that for impedance, tilt and ellipticity, the full-space model gives an excellent approximation to the half-space results (e.g., Fig 4 and 8 are typical even at very shallow depth).

The computer time for the full-space approximate solutions is orders of magnitude faster than the complete solution, mainly achieved by not calculating the surface reflections that involve the infinite sums. Thus the approximate solution is useful in an iterative inversion. A MATLAB code, keyed to the equations in this paper, that reproduces the dashed lines in Figures (4-8), is included in the supplementary material.

As examples of application of the above theories, in the following section we fit the model to VLF tilt data measured above a magma-filled dike that intruded into the flank of Kilauea volcano in 1973 and were published by Zablocki (1976,1978) and above a dike on the south flank of Mt. Etna, Sicily, that intruded in 2001 (Bonaccorso et al., 2002).

4 Field Examples

4.1 Kilauea East Rift Zone, Hawaii

On May 5 1973 an eruption occurred in Hi'iaka and Pauahi craters located in Kilauea's east rift zone on the island of Hawaii (Klein et al., 1987; Tilling et al., 1987). Con-

temporaneously a 100m-long eruptive fissure developed about 1 km west of Hi'iaka Crater and electromagnetic surveys were used to infer that the associated magma intrusion extended a further 2 km as an underground dike (Zablocki 1976). VLF surveys were made along 6 profiles that crossed the dike, and showed characteristic positive followed by negative peaks in the tilt field separated by about 100 m.

Dikes in Hawaii are thought to reach to depths of km. The skin depth in Hawaii is about 300m. Because they have dimensions greater than several skin depths, remainder terms as in Eq(41) were included. We fixed a=1000 m, since for dimensions above several skin depths the model is insensitive to the deeper termination. We also fixed width=1m and conductivity of the magma $\sigma_2 = 1S/m$, since conductivity-contrast times width trade off against each other. We carried out a non-linear inversion for the parameters: conductivity of the surrounding medium, location, depth, and dip. Also, because the measured field showed skewness, we included, as an unknown, the background tilt of the incident magnetic field Φ_0.

The resulting fit {$\sigma_1 = 1.62 \pm 0.04 \times 10^{-4}$ S/m, Depth=17.2 $\pm$ 0.57 m, $\theta = 82 \pm 3^o$, Φ_0=5.7 $\pm$ 0.5 % is shown in Figure (9). As expected we found the fit was independent of the lower depth extent of the dike. A more extensive model may be required to address the non-uniqueness of this type of inversion, but we conclude that the data are fit by a near-vertical dike of depth 17 m containing molten basalt. Both full-space and half-space models were used in the inversions. As expected from the tilt curves in Figure (4), the results were sufficiently similar to justify using the simpler full-space equations (Eq. 41) in the inversion.

4.2 Mt. Etna, Sicily

Beginning on 12 July 2001 seismic activity, GPS and tiltmeter measurements indicated that a dike was intruding into the south flank of Mt Etna, which culminated in an eruption on July 17. Surface non-magmatic fissures indicated the path of the intrusion. Inversion of the geodetic data described a dike running approximately north-south, with a vertical extent of about 2.5 km and opening of 3.5 m (Bonaccorso et al., 2002).

In May 2003 we conducted a VLF survey west to east across the fissure zone (Figure 10) at an elevation of 2186 m. The data were noisy, and as a check, two surveys were carried out. The VLF tilt field from both, shown in Figure (10), is highly unevenly distributed about zero. We thus assumed, like in the Hawaii case , that a background regional tilt was present, but significantly larger.

The data were inverted (Figure 10) based on Eqs.(41, 49); σ_2, w, and a were fixed as $\sigma_2 = 1$ S/m; w=3.5m, and a=1000 m. The inversion for the remaining parameters gave $\sigma_1 = 5.1 \pm 0.72 \times 10^{-4}$ S/m, Depth=20.1 $\pm$ 3.1 m, $\theta = 36 \pm 5^o$, Φ_0=36 $\pm$1% .

The skin depth on Etna is 171 meters. The dip of the dike does not correspond to the vertical dike found geodetically. However the VLF is most sensitive to the upper several hundred meters. The combination of near-surface dip and a deeper vertical dike may account for the regional dip Φ_0. Such a composite model is beyond the scope of this paper. Again, both full and half-space models gave similar results.

5 Discussion and Conclusions

We have applied the Galerkin-Chebyshev matrix method to solve for the induced field in a conductive strip embedded in a conductive medium subjected to electromagnetic radiation. A simple full-space model given by Eq.(35) is both fast and sufficiently accurate for inverting tilt and ellipticity measured over buried dipping dikes. A MATLAB program is suppled in the supplementary material that can be modified for general inversion.

For the infinite medium, and infinite skin depth, and a particular conductivity distribution, the solution converges to Parker's analytic solution. Parker's (2011) solution used the Schmidt-Hilbert method (Porter and Stirling, 1993) to separate the kernel of the integral equation. Based on his approach, we find here that an equivalent method of expanding the kernel in a Chebyshev spectrum gives the same result. Its simplicity arises because of his choice of the singular conductivity function that corresponds to the weight function for orthogonality of Chebyshev polynomials. Thus, in that case, the 2D Chebyshev spectrum is a diagonal matrix that has a simple inverse.

For more general conductivity, the spectrum has off-diagonal terms that may either be calculated as analytical series, or by using a modified fast Fourier transform. Then a matrix inversion needs to be carried out to obtain the final series solution. By separating out the logarithmic singularity from the modified Bessel function kernel, the combined 2D Chebyshev spectrum can be calculated as the sum of the closed-form logarithmic spectrum and numerical evaluation of the non-singular remainder. For skin depths greater than the dimensions of the body the remainder is of second order, and the closed-form logarithmic spectrum suffices.

The half-space model, including surface reflections, and convolution of Green's functions to obtain surface fields, was also solved using Chebyshev spectra. Any two-dimensional cross-section can be analyzed in this way. The most time-consuming calculations are the infinite sums for the surface reflections. However, for a given range of surface locations and depth, this required one evaluation at Chebyshev-Gauss-Lobatto locations to obtain spectral components that then can be evaluated anywhere within that volume during an inversion.

The approximate (full-space) solution has some advantages over numerically solving the integral equation, since it avoids problems associated with digitizing the logarithmic singularity, is computationally faster, and provides simple equations against which numerical schemes can be checked. The use of Chebyshev-Gauss-Lobatto nodes concentrates the digitization near the ends of the strip where the induced field variation is greatest (e.g., Fig. 2). Chebyshev polynomials are near-minimax approximations to a given function, i.e. they minimize the maximum error. In addition the expansion can be truncated at frequencies above which the problem is not resolved. The surface fields then obtained are continuous across the surface rather than at discrete points as given by numerical methods. The full solution requires including surface reflections, but for all the cases we have tested for tilt, impedance and ellipticity, these effects are small.

As examples we show the inverted fits of the model to tilt data measured above a magma-filled dike that intruded in Hawaii, in 1973 and Mt. Etna in 2001. Either full or half-space inversions gave similar results. The inversions gave the location, depth, dip, that correspond to values seen in exposed dikes and conductivities that are consistent with measured properties of solid and molten basalt.

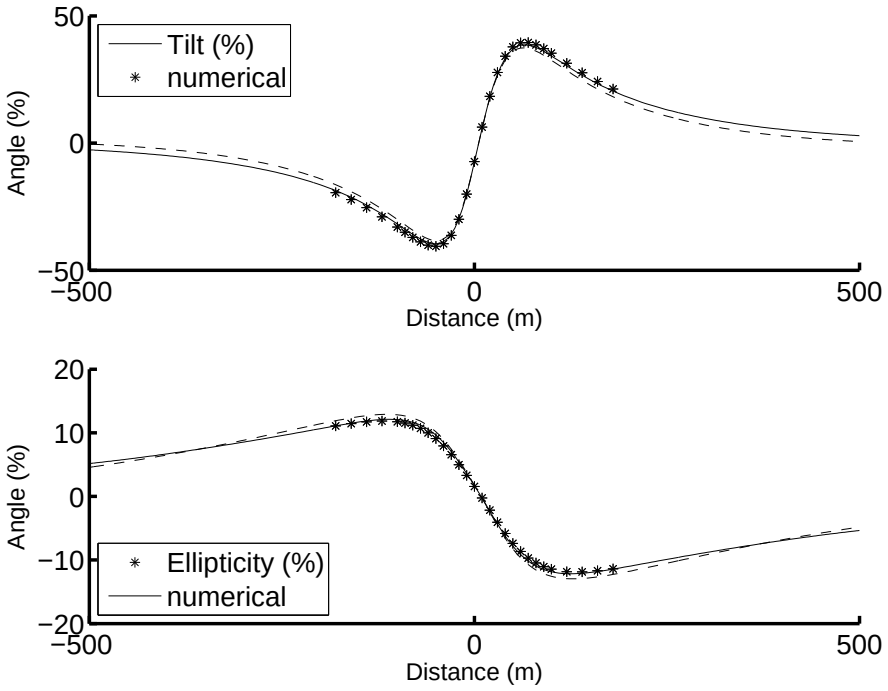

Figure 4: Tilt and ellipticity for a model that is similar to one published by Zablocki, (1976), i.e., $\sigma_1 = 0.0001, \sigma_2 = 1$ S/m, Depth=30 m, Width=1 m, Length=25 m, but with a dip of 60^o. Stars are numerical solutions using a MATLAB version of the FORTRAN program SCATPW.F90 described by Anderson et al., (1976). For compatibility with that program the incident field at the surface was taken to be $H_x = -5.3076$ T which corresponds to an incident E field of 2000 v/m. Solid lines are half-space solutions (Eq. 61) including surface terms. Dashed lines use the approximate Eq.(61) excluding surface terms.

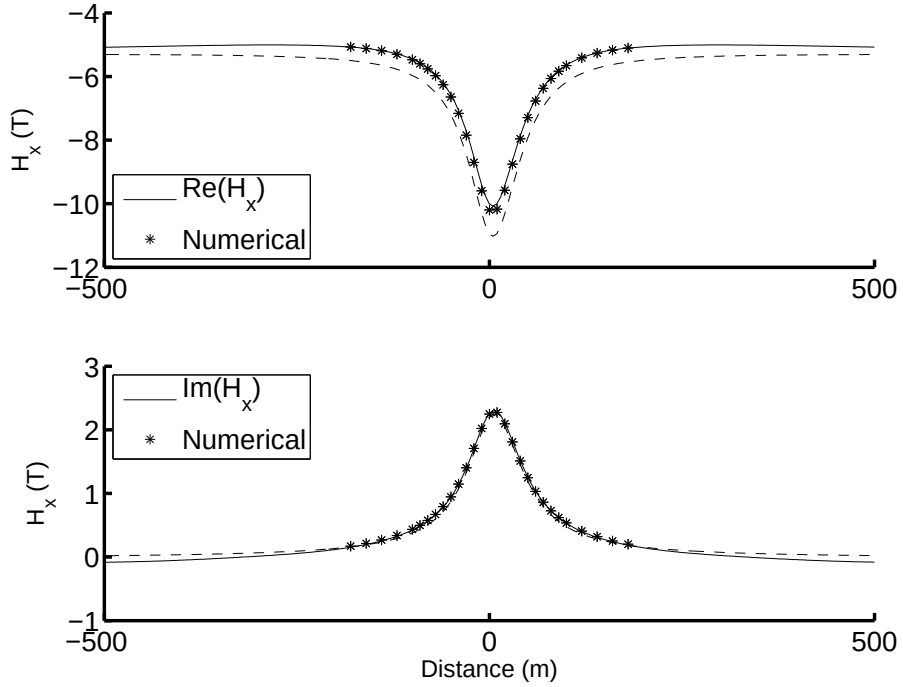

Figure 5: Real and imaginary H_x for the model described in Figure 4.

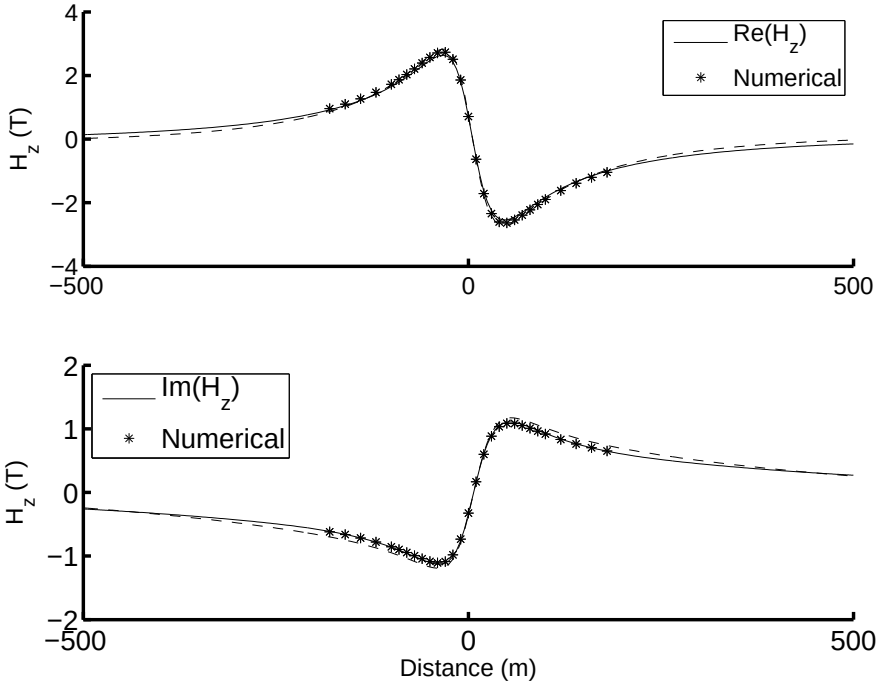

Figure 6: Real and imaginary H_z for the model described in Figure 4.

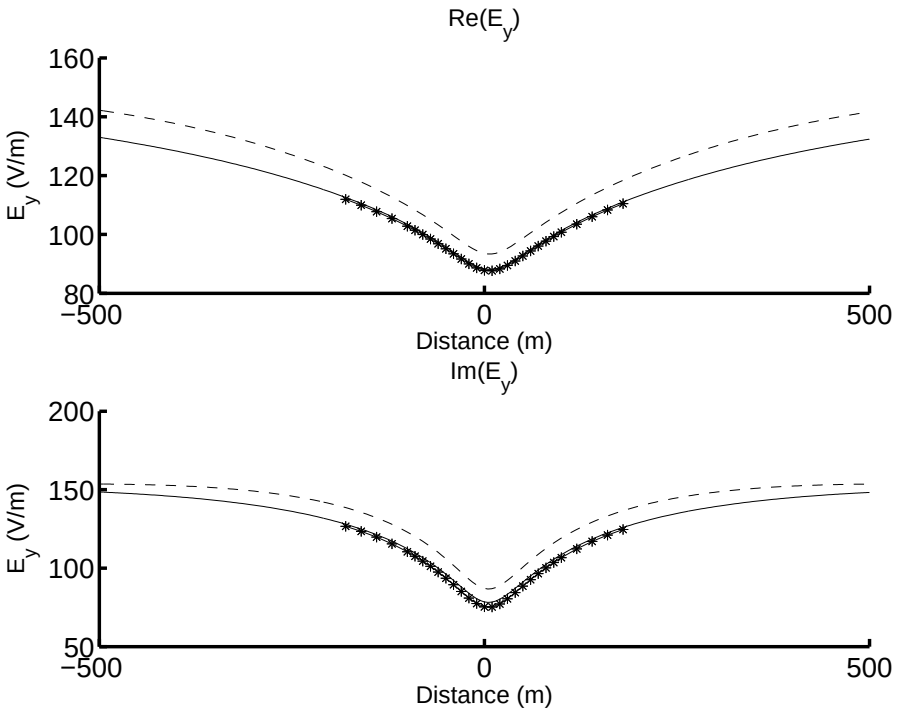

Figure 7: Real and imaginary E_y for the model described in Figure 4.

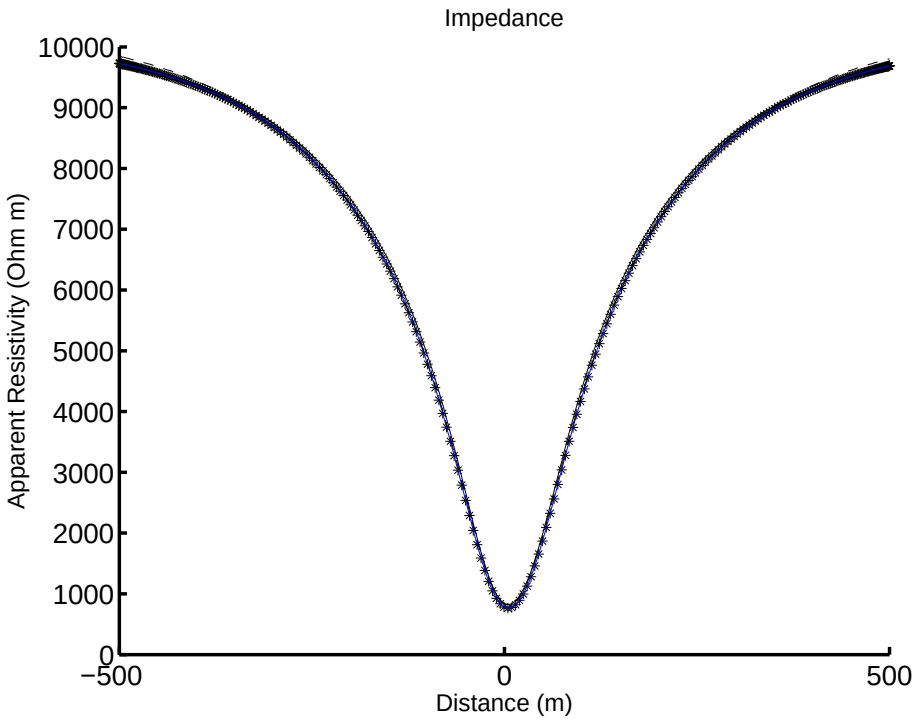

Figure 8: Impedance for the model described in Figure 4.

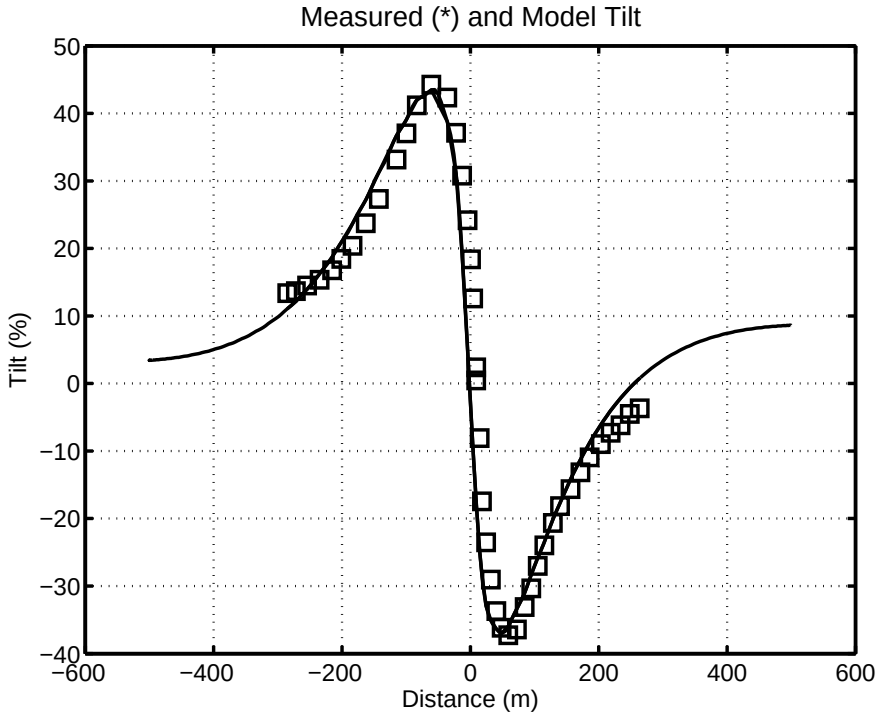

Figure 9: A fit to the measured VLF tilt above the Hi'iaka dike in Hawaii that intruded over a distance of several km in Kilauea's East Rift Zone in 1973 (as reported by Zablocki, 1976). The fitting function was based on Eq.(61). Both full and half-space models gave a similar fit

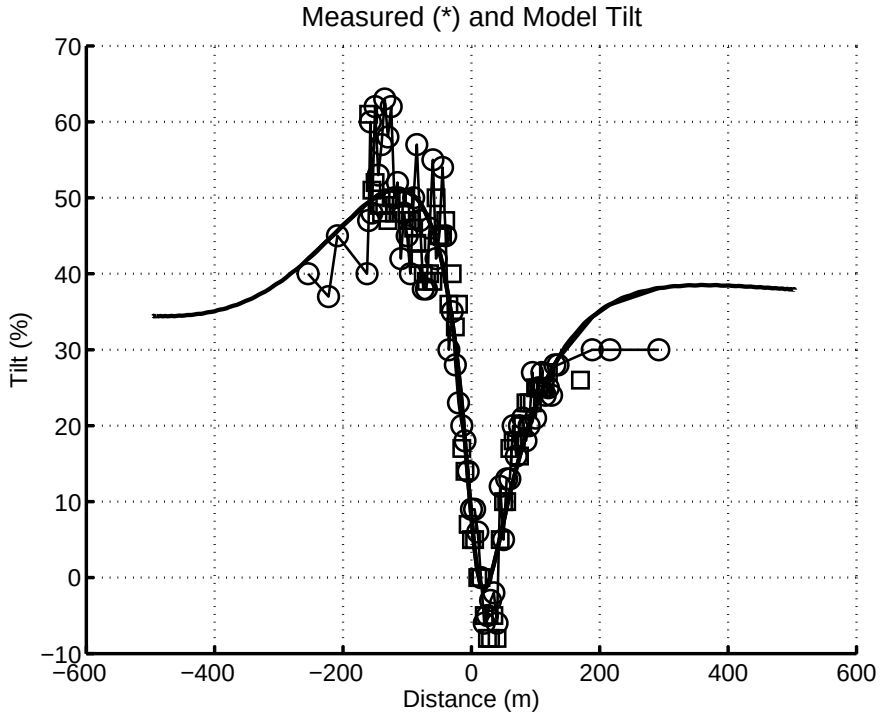

Figure 10: A fit to the measured VLF tilt above a dike that intruded into Etna volcano in 2001. Squares and circles give results of two independent surveys. The fitting function was based on Eq.(61). Both full and half-space models gave a similar fit

6 Acknowledgements

Helpful reviews from Robert Parker and an anonymous reviewer are gratefully acknowledged. Members of the INGV Volcano Observatory in Catania, and its Director Alessandro Bonaccorso are thanked for facilitating the VLF survey on Mt. Etna. The UCLA geophysics class of 2003 is thanked for assisting in the VLF survey on Mt. Etna along with UCLA Profs. McPherron and Tackley. James Kauahikaua of Hawaiian Volcano Observatory is thanked for providing the author a copy of SCATPW.F90.

7 References

Abramowitz, M., and Stegun, I.A., 1972. Handbook of Mathematical Functions, Mathematics Series 55 (National Bureau of Standards, Washington, DC.,1972).

Anderson, L.A., Hohmann, G.H., and Smith, B.D., 1976. Electromagnetic scattering by multiple conductors in the earth due to a plane wave source. U. S. Geol. Surv. Rep. USGS-GD-76-019, 25 pp., available from U.S. Dep. of Commerce, Natl. Tech. Inf. Service Springfield, Va. 22161 as Rep. PB-261-183/AS.

A. Bonaccorso, M. Aloisi and M. Mattia, 2002. Dike emplacement forerunning the Etna July 2001 eruption modeled through continuous tilt and GPS data Geophys. Res. Letters, DOI: 10.1029/2001GL014397.IN 2001 a dike intruded into the southern flank of Mt. Etna.

Boyd, J.P., 2001. Chebyshev and Fourier Spectral methods, 2nd edition, Dover Publication, Inc., Mineola, New York.

Cope, D. K., 1998. Recursive generation of the Galerkin-Chebyshev matrix for convolution kernels, Advances in Comp. Math., 9, 21-35.

Hohmann, G.W., 1971. Electromagnetic scattering by conductors in the Earth near a line source of current, Geophysics 36, 1, 101-131.

Klein, F.W., Koyanagi, R.Y., Nakata, J.S., and Tanigawa, W.R., 1987. The seismicity of Kilauea's magma system, in Decker, R.W., Wright, T.L., and Stauffer P. H., (eds.), 1987, Volcanism in Hawaii: U.S. Geological Survey Professional Paper 1350, p. 1019-1185.

Kauahikaua, J.P., Cashman, K.V., Mattox, T.N., Heliker, C.C., Hon, K.A., Mangan, M.T., and Thornber, C.R.,1998. Observations on basaltic lava streams in tubes from Kilauea Volcano,island of Hawai 'i:Journal of Geophysical Research,v.103,no.B11, p.27303 –27323.

Key, K. and Weiss, C., 2006. Adaptive finite-element modeling using unstructured grids: The 2D magnetotelluric example, Geophysics, 71(6), G291-G299. doi: 10.1190/1.2348091.

Parker, R.L., 2011. New analytic solutions for the 2D-TE mode MT problem, Geophys. J. Int., 186, 980-986.

Porter, D., and Strirling, D.S.G., 1990. Integral Equations, Cambridge University Press, Cambridge.

Rankin, D., 1962. The magneto telluric effect on a dike, Geophysics, 27, 5, 666-676.

Telford, W.M., L.P. Geldart, and R.E. Sheriff, 1990. Applied Geophysics, Second Ed. Cambridge University Press., 770 pp.

Tilling, R.I., Christiansen, R.L., Duffield, W.A., Endo, E.T., Holcomb, R.T., and Koyanagi, R.Y., Peterson, D.W., and Unger, J.D., 1987, The 1972-1974 Mauna Ulu eruption, Kilauea Volcano: an example of quasi-steady-state magma transfer, in Decker, R.W., Wright, T.L., and Stauffer P. H., (eds.), 1987. Volcanism in Hawaii: U.S. Geological Survey Professional Paper 1350, p. 405-469.

Von Winckel, G., 2004. 2D Chebyshev Transform fclgtran2d.m, Matlab Central, Copyright (2009) by Greg Von Winckel.

Wait, J.R., 1962. Electromagnetic waves in stratified media, New York, MacMillan.

Wannamaker, P. E., J. A. Stodt, and L. Rijo, 1987. A stable finite-element solution for two-dimensional magnetotelluric modeling: Geophysical Journal of the RoyalAs-

tronomical Society, 88, 277–296.

Weaver, J., B. LeQuang, and G. Fischer, 1985. A comparison of analytic and numerical results for a two-dimensional control model in electromagnetic induction, Part I, B-polarization calculations: Geophysical Journal of the RoyalAstronomical Society, 82, 263–277.

Weaver, J., B. LeQuang, and G. Fischer, 1986. A comparison of analytical and numerical results for a 2-d control model in electromagnetic induction, Part II, E-polarization calculations: Geophysical Journal of the Royal Astronomical Society, 87, 917–948.

Zablocki, C. J., 1976. Mapping thermal anomalies on an active volcano by the self-potential method, Kilauea, Hawaii, In: Proc., 2nd U.N. Symposium on the Development and Use of Geothermal Resources, San Francisco, Calif., May 1975, 2: 1299-1309.

Zablocki, C. J., 1978. Applications of the VLF induction method for studying some volcanic processes of Kilauea volcano, Hawaii, J. Volcanol. and Geothermal Res., 3, 155-195.